1998

Observations of BL Lacertae from the Geodetic VLBI Archive of the Washington Correlator

C. E. Tateyama

K. A. Kingham

P. Kaufmann

B. G. Piner
Whittier College, gpiner@whittier.edu

A. M. P. de Lucena

See next page for additional authors

THE ASTROPHYSICAL JOURNAL, 500:810–815, 1998 June 20

OBSERVATIONS OF BL LACERTAE FROM THE GEODETIC VLBI ARCHIVE OF THE WASHINGTON CORRELATOR

C. E. TATEYAMA
Centro de Rádio-Astronomia e Aplicações Espaciais (CRAAE), Escola Politécnica da Universidade de São Paulo, CP61548, 05424-970, São Paulo, SP, Brazil

K. A. KINGHAM
US Naval Observatory, Earth Orientation Department, 3450 Massachusetts Avenue, Washington, DC 20392

P. KAUFMANN
Centro de Rádio-Astronomia e Aplicações Espaciais (CRAAE), NUCATE/UNICAMP, Cidade Universitária, 13083-592, Campinas, SP, Brazil

B. G. PINER
US Naval Observatory, Earth Orientation Department, 3450 Massachusetts Avenue, Washington, DC 20392; Department of Astronomy, University of Maryland, College Park, MD 20742; and NASA Goddard Space Flight Center, Code 661, Greenbelt, MD 20771

A. M. P. DE LUCENA
ROEN, Rádio Observatório Espacial do Nordeste, CRAAE/INPE, Estrada do Fio, 6000, Eusébio, Fortaleza, CE, Brazil

AND

L. C. L. BOTTI
Centro de Rádio-Astronomia e Aplicações Espaciais/CRAAE, Escola Politécnica da Universidade de São Paulo, CP61548, 05424-970, São Paulo, SP, Brazil

Received 1997 October 21; accepted 1998 January 28

ABSTRACT

We present maps of BL Lac obtained from geodetic VLBI data from the archive of the Washington correlator. The observations were made from 1996 March to 1996 November, with periods from one experiment to another as short as 1 month. The dominant structure of the maps is given by a superluminal component (C2) moving predominantly at position angle $\sim 190°$. At the later epochs a new superluminal component (C3) emerges from the core and moves along a trajectory at a higher position angle (200°). We also include maps from observations made in 1995 June and August showing the main component (C2) in the early stages of its evolution, as well as an older component (C1). The position angle of the component C1 is nearly the same as that of the new component C3. The component C2 shows indications of nonradial motion, which is discussed in terms of a helically distorted jet. The best fit was obtained for a half–opening angle of the jet of 2°.6 and an angle of the helical axis to the line of sight of 17°.

Subject headings: BL Lacertae objects: individual (BL Lacertae) — galaxies: jets — radio continuum: galaxies — techniques: interferometric

1. INTRODUCTION

BL Lac is a well-known superluminal source exhibiting high proper motion. In a year a knot moves about 1 mas on the sky. At $z = 0.069$ (Miller, French, & Hawley 1978), this corresponds to an apparent velocity of $3.2\ h^{-1}\ c$ for a Hubble constant $H_0 = 100\ h$ km s^{-1} Mpc^{-1} and $q_0 = 0.5$. In the framework of bulk relativistic motion, the observed properties of the source are very dependent upon the jet orientation to the line of sight. In the case of BL Lac, there is a general acceptance that the jet is viewed at a rather high angle to the line of sight. Mutel et al. (1990) using VLBI data interpreted the moving components as shocked-jet features propagating with a velocity only modestly larger than that of the underlying flow ($\gamma \sim 4$), and deduced a viewing angle which could not be less than 19° to account for geometrical constraints dictated by the size of the VLBI components. A similarly large viewing angle was needed by Hughes, Aller, & Aller (1989) to explain the shape of the light curves of total flux and polarized flux. A flow of Lorentz factor $\gamma \sim 6$ was modeled with a viewing angle of 38° to reduce the percentage of polarization of the outburst.

The motion of the superluminal components is mostly rectilinear, southward at position angle (P.A.) ranging from 190° to 200° (Mutel et al. 1990; Mutel, Denn, & Dryer 1994). In fact, early VLBI components designated S1, S2, and S3 by Mutel et al. (1990) have a predominant P.A. near 190°, while more recent VLBI components (S5 and S6) have a P.A. of about 200°. This shift of jet orientation has led Mutel et al. (1994) to suggest a precession of the central engine under the influence of a massive companion, so that the spin axis of the bulk relativistic motion where shocks propagate changes over time. A corresponding shift of 10° of the P.A. of the polarization was also reported by Aller, Hughes, & Aller (1994) for the same time periods.

The present data consist of geodetic VLBI observations at 8.5 GHz archived at the Washington correlator. There are 10 epochs of VLBI observations, which were obtained between 1995 June and 1996 November. Geodetic VLBI maps have been successfully used for astrophysical studies of compact sources (e.g., Guoquiang, Rönnäng, & Bååth 1987; Charlot 1990; Britzen et al. 1994; Vicente, Charlot, & Sol 1996). More recently, Piner & Kingham (1997) obtained a series of good-quality images of the blazar 1611+343 from the Washington VLBI correlator's database.

2. OBSERVATIONS

The VLBI observations used in this paper are from geodetic VLBI data archived at the Washington correlator. These data were obtained from the geodetic dual-frequency VLBI experiments (Rogers et al. 1983) carried out by the

TABLE 1

8.4 GIGAHERTZ VLBI OBSERVATIONS OF BL LAC

Epoch	Name	Antennas[a]	Synthesized Beam (mas × mas)	Beam Angle (deg)	Number of Scan Baselines
1995 Jun	NAEXS6	GAMWOV	1.02 × 0.61	−15	90
1995 Aug	NA118	FKMWK	0.68 × 0.37	12	54
1996 Mar	NA152	FAKNOV	0.53 × 0.48	52	99
1996 Apr	NAEXS10	GAKNOV	1.04 × 0.67	5	21
1996 May.....	NA159	GFAKNV	0.54 × 0.52	16	68
1996 Jun	NA164	GFAKNV	0.63 × 0.52	17	51
1996 Jul.....	NA168	FAKNV	0.63 × 0.43	39	54
1996 Sep	NA175	FAKNOV	0.58 × 0.51	30	125
1996 Oct.....	NA180	FKNV	0.61 × 0.38	7	46
1996 Nov	NA185	FAKNOV	0.56 × 0.52	20	101

[a] A = Gilcreek (Alaska; 26 m), F = Fortaleza (Brazil; 14 m), G = Algopark (Ontario; 46 m), K = Kokee (Hawaii; 20 m), N = NRAO (Green Bank; 20 m), M = Miami (20 m), O = Ny Alesund (Norway; 20 m), V = Wettzell (Germany; 20 m), W = NRAO85 (Green Bank; 26 m).

US Naval Observatory (Eubanks et al. 1991), the National Oceanographic and Atmospheric Administration (NOAA) (Carter, Robertson, & MacKay 1985), the Crustal Dynamics Project, and the Space Geodesy Project (Coates et al. 1985; Smith & Turcotte 1993). The VLBI observations were processed at the Washington VLBI Correlator at the US Naval Observatory (USNO).

All observations were carried out with the Mark III dual-frequency VLBI receivers in both the X and the S band (centered at 8.5 and 2.3 GHz, respectively), providing noise temperatures of 70–200 K. The X band consists of eight individual channels of 2 MHz width, spanning frequencies from 8.2 to 8.9 GHz. Almost all stations were equipped with H masers as the local frequency standard.

BL Lac is one of most densely observed geodetic sources; however, only since 1995 have useful visibility data for imaging become available. Table 1 lists the epochs of observation, names of the experiments, antennas participating on the network, interferometric dirty beams, and the number of scan baselines in the observation. The dirty beams were about 0.5–0.6 mas for all maps, except for the first and fourth experiments. We have used a restored circular beam of 0.5 mas on the maps. The dynamic range, defined as the ratio of the peak flux per beam to the lowest positive contour in the maps, is about 250:1.

The fringe fitted data were coherently averaged to 4 s to determine the visibilities. The data were calibrated and fringed using standard routines from the AIPS software package, and the images were produced using the self-calibration procedures (e.g., Pearson & Readhead 1984) of the Caltech Difmap software. Piner & Kingham (1997), also using the geodetic VLBI data from the Washington correlator, found an error in the absolute flux density as low as 8% at 8 GHz.

3. RESULTS AND DISCUSSION

The 8 GHz maps are presented in Figure 1. The maps show a core-jet structure with superluminal components moving southward. The detection of the prominent components appears to be limited to a distance not much farther than 2 mas from the core. Beyond this point the brightness of the components is below the sensitivity of the present network. Similar results are seen in the 10 GHz VLBI observations of Mutel et al. (1990). Table 2 lists the fluxes and positions of the components for each image. All components were fitted using a circular Gaussian model. Figure 2 shows the sequence of maps from all epochs to illustrate the change of the structure as the superluminal components move southward with time. The main superluminal component (C2) moves along a trajectory at P.A. 190°. At later epochs a new component (C3) starts to dominate the structure. The position angle of C2 in our maps, which corresponds to the component S8 in the nomenclature of Mutel et al. (1990), does not differ much from that of the component S1 seen 16 years ago. In fact, the measured position angles of earlier VLBI components indicated a jump of the position angle from a given component to another rather than a gradual continuous change of the jet orientation, viz., the components S1, S2, and S3 appeared to move along the same trajectory at P.A. 190°, and the components S4, S5, and S6 appeared to move at P.A. 200°. In addition to the components C2 and C3, an older component C1 can be seen at earlier epochs. Similarly to C3, C1

TABLE 2

BL LAC AT 8 GIGAHERTZ[a]

Epoch	Component	Flux (Jy)	r (mas)	P.A. (deg)	θ (mas)
1995 Jun	Core	1.07	0.00	0	0.03
	C2	0.58	1.04	183	0.04
	C1	0.48	1.63	203	0.55
1995 Aug	Core	1.44	0.00	0	0.04
	C2	0.96	1.11	176	0.20
	C1	0.11	1.80	199	0.01
1996 Mar	Core	1.27	0.00	0	0.18
	C2	2.09	1.42	188	0.44
1996 Apr	Core	1.46	0.00	0	0.01
	C2	1.85	1.64	191	0.65
1996 May.....	Core	2.00	0.00	0	0.17
	C2	1.91	1.78	192	0.69
1996 Jun	Core	1.73	0.00	0	0.01
	C2	1.51	1.89	192	0.64
1996 Jul.....	Core	2.30	0.00	0	0.06
	C2	0.35	1.92	196	0.02
1996 Sep	Core	1.69	0.00	0	0.07
	C3	0.92	0.53	212	0.02
	C2	0.95	2.05	194	0.44
1996 Oct.....	Core	1.69	0.00	0	0.06
	C3	0.88	0.80	201	0.06
	C2	0.94	2.09	192	0.40
1996 Nov	Core	2.42	0.00	0	0.21
	C3	1.17	1.06	206	0.44
	C2	1.00	2.20	192	0.60

[a] P.A. is the position angle of the component at radius r, and θ is the Gaussian circular size.

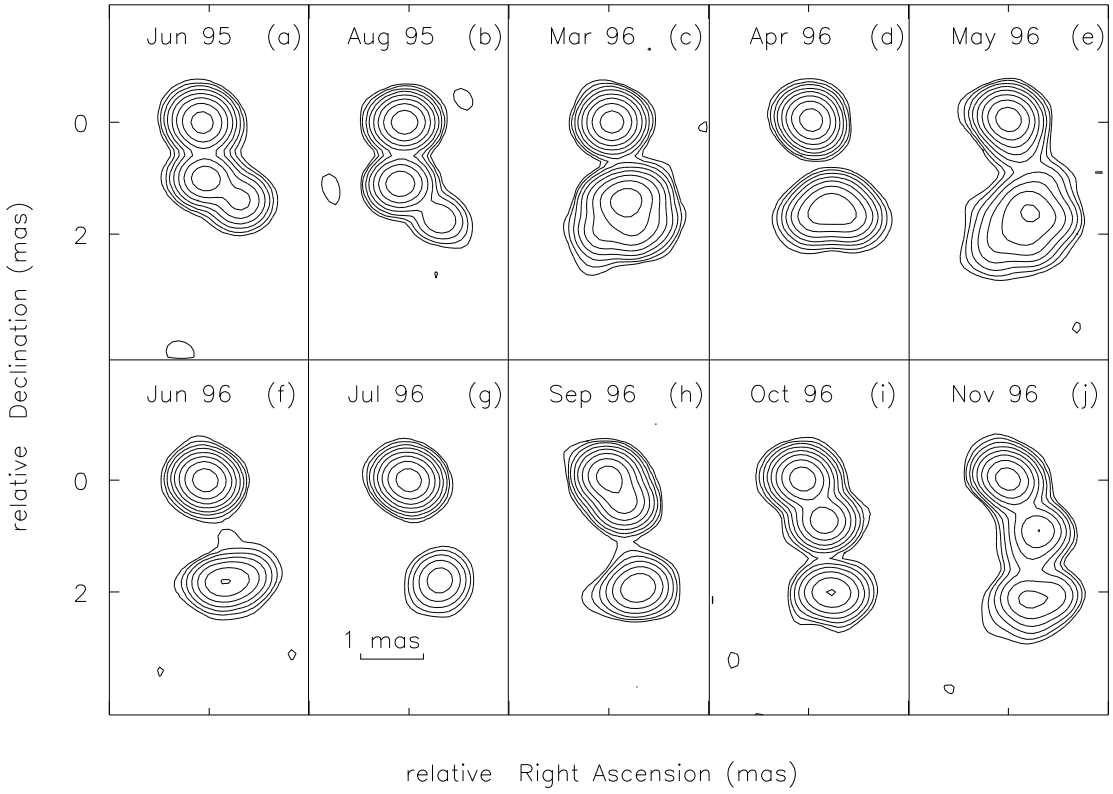

FIG. 1.—(*a–j*) 8 GHz VLBI maps of BL Lac. Contour levels are −0.5, 0.5, 1, 2, 4, 8, 16, 32, and 64 percent of the peak brightness. The peak brightnesses of the maps are 1.18, 1.40, 1.25, 1.49, 1.86, 1.81, 2.29, 1.81, 1.65, and 2.15 Jy beam^{-1}, respectively. The restored circular beam is 0.5 mas.

appears at P.A. 200°, suggesting that the trajectory of each knot may alternate between P.A. 190° and P.A. 200° from a given knot to another on a timescale of less than 2 years. This period is too short to be ascribed to a precession of a body of mass $\sim 10^8\ M_\odot$ (Begelman, Blandford, & Rees 1980). The outer components of the maps made in 1995 July and August appear as an extended component comprising the components C2 and C1. The separation between C2 and C1 is only 0.6 mas, which is about equal to or less than the beam size. A fit of the component positions with time from 1996 March to 1996 November results in a reasonably good fit to a straight line, with an angular separation rate of 1.1 mas yr^{-1} for C2 (apparent velocity of 3.6 $h^{-1}\ c$). However, the line falls well below the data for the early observations of C2, in1995 July and August. This indicates a stage of rapid expansion, along with a small contraction during the gap between 1995 August and 1996 March, followed by a slower and constant expansion from 1996 March to 1996 November. The new component C3 is clearly seen separating from the core in 1996 September and November. A fit to the measured positions of C3 implies that this component has a larger expansion speed than C2. However, a blending with the core could shift the apparent position of this component, and affect the fitted velocity.

3.1. *Helical Motion*

The sky positions of component C2 are plotted in Figure 3. The valley-shaped appearance of the points around 1995

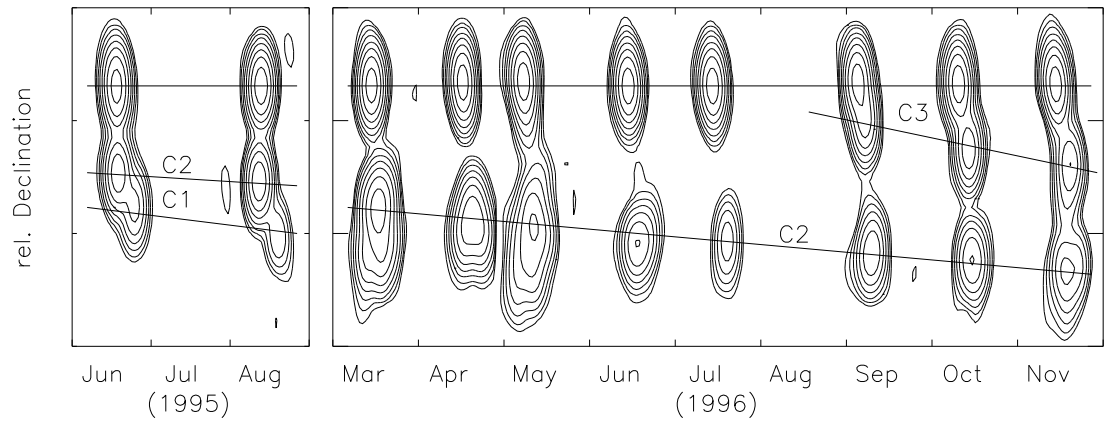

FIG. 2.—Time sequence of the maps showing the motion of the components. Time is plotted along the horizontal axis, and relative declination is plotted along the vertical axis. The northernmost component is assumed to be the stationary core. The moving components are labeled C1, C2, and C3. The maps are stretched out vertically to emphasize the moving components.

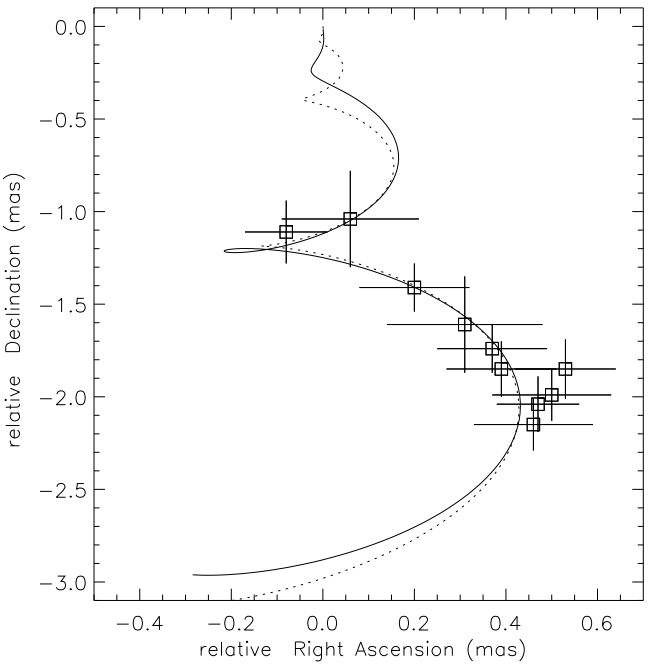

FIG. 3.—Sky positions of component C2 superposed with sky positions derived from the adiabatic model (*solid line*) and isothermal model (*dotted line*). Our estimated conical helix has been rotated 87° (isothermal) or 88° (adiabatic) clockwise in order to coincide with the sky positions of component C2. The uncertainty is assumed to be one-quarter of the beamwidth.

August and 1996 March suggests the presence of a loop, such as that which would be described by a moving feature in helical trajectory. Such bent trajectories of moving features have been seen frequently, and have been interpreted as evidence of helical motion in various superluminal sources (e.g., Steffen et al. 1995; Qian et al. 1996). In particular, a hydrodynamically generated helical jet model developed by Hardee (1987) has been applied to the radio structure of 3C 345 (Hardee 1987). Vicente et al. (1996), using geodetic VLBI data, obtained a fit to a helical model with two consecutive loops for OJ 287. A geometry in which the helical distortions saturate far from the core has been used to explain the orthogonal parsec-scale and kiloparsec-scale jet structure observed in some sources (Conway & Murphy 1993), such as Mrk 501 (Conway & Wrobel 1995).

In what follows, we consider the hydrodynamical helical jet model described by Hardee (1987). In cylindrical coordinates the helical trajectory can be described by the amplitude A in the radial direction and by the phase angle ϕ with respect to the z-axis. The helical axis is oriented along the z-axis, at an angle χ to the observer's line of sight. The observer is in the y-z plane, and the x-axis is in the plane of the sky. For the adiabatic expanding jet the phase angle and amplitude are given by

$$\phi = \frac{4\pi R_1}{\Psi\lambda_1}\left[1 - \left(\frac{R}{R_1}\right)^{1/2}\right] + \phi_1 , \quad (1)$$

$$A = A_1 \exp\left\{2d_1\left[1 - \left(\frac{z_1}{z}\right)^{1/2}\right]\right\}, \quad (2)$$

where $R = z\Psi + R_0$; Ψ is the half–opening angle of the jet; $R_0 = z_0\Psi$ is the initial jet radius evaluated at the origin of the cone, z_0; A_1, ϕ_1, R_1, and λ_1 are the amplitude and phase of the helix, the radius of the jet, and the helical wavelength, respectively, at a distance $z = z_1$ from the core along the helical axis; d_1 is also evaluated at z_1 and expresses the rate at which the helical amplitude grows. As in Hardee (1987), we have set $A = \alpha R$, i.e., we assume that the ratio α between the amplitude of the helix A and the radius of the jet R is constant.

Figure 3 shows the sky positions of component C2 superposed with the sky projection of the helical jet model. The error in the component positions is taken to be one-quarter of the beam FWHM. The fit was obtained for $\Psi = 2.^\circ6$, $R_0 = 0.023$ mas, $z_0 = 0.5$ mas, $R_1 = 0.118$ mas, $\lambda_1 = 3.48$ mas, $A_1 = 0.13$ mas, $\phi_1 = 0.^\circ0$, $z_1 = 2.1$ mas, $d_1 = 1.1$, $\alpha = 1.1$, and $\chi = 17°$. Our estimated conical helix was rotated 88° clockwise, so that it would coincide with the sky positions of component C2. There is good agreement between the helical path and the observed sky positions. Figure 4 shows that the agreement between the observed and the calculated radial separations of the component with time is also satisfactory. The best fit was obtained with a Lorentz factor of 5. In the case of the isothermal model, the phase angle and amplitude of the helix are given by

$$\phi = \frac{2\pi R_1}{\Psi\lambda_1}\ln\left(\frac{R}{R_1}\right) + \phi_1 , \quad (3)$$

$$A = A_1\left(\frac{z}{z_1}\right)^{d_1} . \quad (4)$$

All parameters have the same meaning as in the adiabatic case. The best fit was obtained for $\Psi = 2.^\circ5$, $R_0 = 0.022$ mas, $z_0 = 0.5$ mas, $R_1 = 0.096$ mas, $\lambda_1 = 1.97$ mas, $A_1 = 0.09$ mas, $\phi_1 = 90°$, $z_1 = 1.7$ mas, $d_1 = 1.0$, $\alpha = 0.9$, and $\chi = 18°$. Our estimated conical helix was rotated 87° clockwise, so that it would coincide with the sky positions of component C2. The fit to the radial separation with time for the isothermal model is not as good as that for the adiabatic model (see Fig. 4). However, if we introduce a variable Doppler

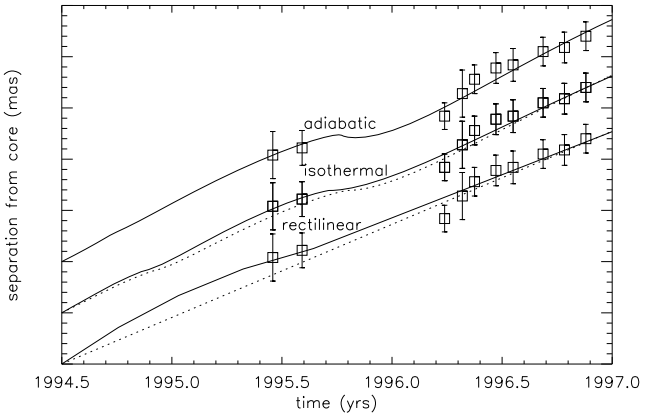

FIG. 4.—Plots from the top to the bottom of the figure represent the radial separation of component C2 with time, superposed with the radial separation calculated from the helical adiabatic, helical isothermal, and rectilinear models. In all cases, the separation from the core at 1994.5 is zero. The separation is plotted with tick-mark spacings of 1 mas. The model curve at the top of the figure shows the adiabatic model using a constant Lorentz factor of 5. The model curves in the middle of the figure show isothermal models using a constant Lorentz factor (*dotted line*), and a variable Lorentz factor that decreases linearly from 4 to 3 in 5 mas along the axis of the helix (*solid line*). The effect of a variable Lorentz factor on the rectilinear motion is also shown at the bottom of the figure (*solid line*). The dotted straight line represents rectilinear motion with a constant Lorentz factor of 3. The uncertainty is assumed to be one-quarter of the beamwidth.

factor into the isothermal model, both models (adiabatic and isothermal) give similar fits to the data. We include in Figure 4, for the sake of comparison, the effect of deceleration on rectilinear motion with an initial Lorentz factor of 4, which decreases linearly to a constant value of 3 in 5 mas along the jet axis. The larger Lorentz factor near the core produces a bump on the curve near the component positions in 1955 July and August. While it is possible to fit the present data reasonably well with both models, the adiabatic model does not require further assumptions about the behavior of the Lorentz factor.

The increase in the flux of component C2 between 1995 July and August, along with its decline after 1996 March (see Table 2), is consistent with the Doppler boosting of this knot as it moves toward and then away from the line of sight along the path given by the helical model fits. Our models predict a local minimum for the apparent speed close to the observed epoch in 1995 August. The relatively low radio flux in 1995 July and August can be attributed to the expansion of the knot as it moves along the helical path.

3.2. *Trajectory of the Components*

An investigation of the trajectory of the components over the years suggests that the components move predominantly at a position angle of either 190° or 200°, rather than exhibiting a continuous change of the position angle as would be expected from jet precession. In addition, while components S2 and S6 show a rectilinear trajectory (Mutel et al. 1994), nonradial motion or simple bending (eastward bending) is present for components S1 and S3. Under such a scenario, BL Lac differs from another BL Lacertae object, OJ 287, where the knots appear to follow the same path (Vicente et al. 1996).

As we have seen, the sky projection of the calculated helix, coupled with the radial separation of component C2 versus time, has provided a fairly good constraint on the jet geometry. Support for these models, especially for the choice of the helical parameters, would be reinforced if it could be shown that previous components exhibited a similar helical pattern. In the following, the same helical model applied to component C2 has been applied to the components S1 and S3. The half–opening angle Ψ, and the angle of the helical axis to the line of sight χ, were the same as those used to fit the helical path of component C2. The only helical parameters that were varied were z_0, z_1, and α. We also kept the pitch angle $\Delta = \arctan(2\pi A/\lambda) =$ constant. The best adiabatic (isothermal) fit for component S1 (see Figs. 5 and 6) was obtained for $z_0 = 2.5$ (0.7) mas, $z_1 = 10.0$ (4.2) mas, and $\alpha = 0.75$ (0.80). In the same way, for component S3 we have $z_0 = 2.8$ (0.8) mas, $z_1 = 8.8$ (3.4) mas, and $\alpha = 0.75$ (0.70). The isothermal fit, for both com-

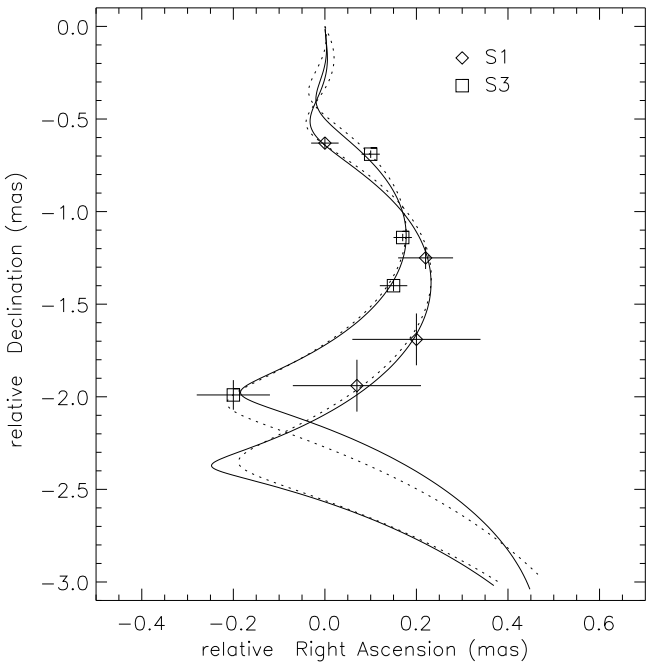

FIG. 5.—Sky positions of components S1 and S3 superposed with the sky positions derived from the adiabatic model (*solid line*) and the isothermal model (*dotted line*). The data are from Mutel et al. (1990).

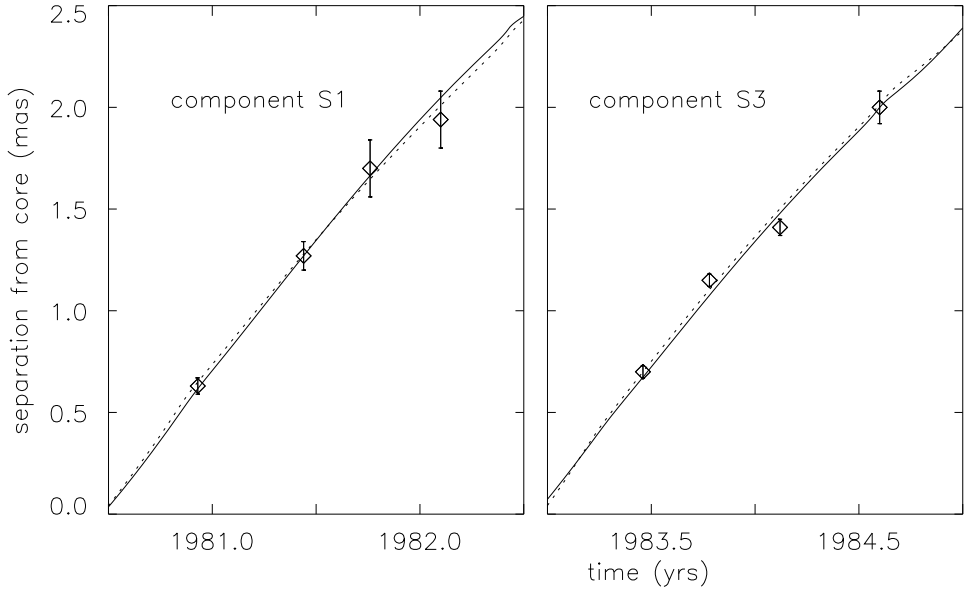

FIG. 6.—Plots represent the radial separation of components S1 and S3 superposed with the derived radial separation from the helical adiabatic (*solid line*) and the helical isothermal (*dotted line*) models. The data are from Mutel et al. (1990).

ponents, was obtained using variable Lorentz factor (from 4 to 3 in 5 mas).

The presence of rectilinear motion, as shown by the older components S2 and S6, may appear somewhat discordant with the helical motions obtained for the other components. However, the helix fitted to the component motions was obtained using a straight jet axis, which is at least an obvious requirement for rectilinear motion. Regardless of the mechanisms responsible to start either helical or rectilinear motion, we may examine whether two different knots moving rectilinearly on the surface of an equivalent cone defined by the helical pattern could be consistent with a separation of $\sim 10°$ between the apparent position angles of components S2 (P.A. = 189°) and S6 (P.A. = 198°). The apparent angle μ between the trajectories is given by (Readhead et al. 1983)

$$\sin(\mu/2) = \sin\varphi \sin\Psi / \sin[\chi - \arctan(\cos\varphi \tan\Psi)] , \quad (5)$$

where Ψ is the half-angle of the cone, χ is the angle between the cone axis and the line of sight, and φ is the azimuthal angle of the trajectory on the cone. We note that the best fits for both the adiabatic and the isothermal models gave similar values for χ and Ψ. For $\chi = 17°$ and $\Psi = 2.^\circ 6$, an apparent angle μ of $\sim 10°$ would correspond to an azimuthal separation angle of $\sim 2\varphi = 80°$, which is satisfactory for knots moving rectilinearly on a conical jet, and, most important, in good agreement with a narrow conical jet.

In summary, our results show that the knots move in a hydrodynamically generated helical pattern along a straight jet axis. The basic jet parameters are given by an angle of the conical axis to the line of sight of 17°, and a half–cone angle of $2.^\circ 6$. The pitch angle of the helical pattern is 12° for the adiabatic model and 17° for the isothermal model. The apparent position angle separation of $\sim 10°$ between two rectilinear trajectories is also consistent with a narrow conical jet. It is encouraging that the basic helix parameters of the component C2 provided an excellent fit to the older components S1 and S3, suggesting that, in addition to the opening angle and the angle of the helical axis to the line of sight, the pitch angle is also unchanged from one knot to another.

C. E. T. thanks the Fundação de Amparo a Pesquisa do Estado de São Paulo for a grant (Proc. 96/6267-1) to undertake 3 months of work with geodetic VLBI data at the US Naval Observatory. He is also grateful to A. C. O. Cancoro de Matos and L. C. L. Botti for installing AIPS; J. E. R. Costa for helping with IDL; and the referee for useful suggestions. The Fortaleza VLBI facility was built and is operated with partial support from the US NOAA, the Brazil Ministry of Science and Technology, MCT-FINEP, and CRAAE (joint center between the Universidade de São Paulo, Mackenzie and UNICAMP Universities, and INPE, Brazil).

REFERENCES

Aller, H. D., Hughes, P. A., & Aller, M. F. 1994, BAAS, 184, 874, n. 11.01
Begelman, M. C., Blandford, R. D., & Rees, M. J. 1980, Nature, 287, 307
Britzen, S., Witzel, A., Gontier, A. M., Schalinski, C. J., & Campbell, J. 1994, in IAU Symp. 159, Multiwavelength Continuum Emission of AGN, ed. T. J. L. Courvoisier & A. Blecha (Dordrecht: Kluwer), 423
Carter, W. E., Robertson, D. S., & MacKay, J. R. 1985, J. Geophys. Res., 90, 4577
Charlot, P. 1990, A&A, 229, 51
Coates, R. J., Frey, H., Mead, G. D., & Bosworth, J. M. 1985, IEEE Trans. Geosci. Remote Sensing, GE-23, 360
Conway, J. E., & Murphy, D. W. 1993, ApJ, 411, 89
Conway, J. E., & Wrobel, J. M. 1995, ApJ, 439, 98
Eubanks, T. M., et al. 1991, in IERS Tech. Note 8 (Paris: IERS), 73
Guoquiang, T., Rönnäng, B., & Bååth, L. 1987, A&A, 185, 87
Hardee, P. E. 1987, ApJ, 318, 78
Hughes, P. A., Aller, H. D., & Aller, M. F. 1989, ApJ, 341, 68
Miller, J. S., French, H. B., & Hawley, S. A. 1978, in Pittsburgh Conf. on BL Lac Objects, ed. A. M. Wolfe (Pittsburgh: Univ. Pittsburgh), 176
Mutel, R. L., Denn, G. R., & Dryer, M. J. 1994, in Proc. NRAO Workshop 23, Compact Extragalactic Radio Sources, ed. J. A. Zensus & K. I. Kellermann (Green Bank: NRAO), 191
Mutel, R. L., Phillips, R., Su, B., & Bucciferro, R. R. 1990, ApJ, 352, 81
Pearson, T. J. & Readhead, A. C. S. 1984, ARA&A, 22, 97
Piner, B. G., & Kingham, A. K. 1997, ApJ, 479, 684
Qian, S. J., Krichbaum, T. P., Zensus, J. A., Steffen, W., & Witzel, A. 1996, A&A, 308, 395
Readhead, A. C. S., Hough, R. C., Ewing, M. S., Walker, R. C., & Romney, J. D. 1983, ApJ, 265, 107
Rogers, A. E. E., et al. 1983, Science, 219, 51
Smith, D. E., & Turcotte, D. L. eds. 1993, Geodynamics Ser. 23, Contributions of Space Geodesy to Geodynamics: Crustal Dynamics (Washington, DC: AGU)
Steffen, W., Zensus, J. A., Krichbaum, T. P., Witzel, A., & Qian, S. J. 1995, A&A, 302, 335
Vicente, L., Charlot, P., & Sol, H. 1996, A&A, 312, 727